Carbon Vol. 24, No. 1, pp. 51–59, 1986
Printed in Great Britain.

0008-6223/86 $3.00 + .00

REACTIVITY AND RELATED MICROSTRUCTURE OF 3D CARBON/CARBON COMPOSITES

L. E. Jones, P. A. Thrower and P. L. Walker, Jr.
Department of Materials Science and Engineering, The Pennsylvania State University, University Park, PA 16802, U.S.A.

(*Received* 9 *May* 1985)

Abstract—Four carbon/carbon composites fabricated with either PAN fibers or coal tar pitch fibers were examined. Detailed analysis of composite properties and structure included total surface area by Kr adsorption at 77 K, active surface area, porosity, crystallite parameters, as well as SEM and optical microscopic observations. Rates of composite gasification were measured at 1123 K in 3.1 kPa of steam. Under these experimental conditions the composites fabricated with PAN fibers are roughly three times as reactive as those fabricated with pitch fibers. Microscopic examination of the composites provides detail on two different microstructures for each fiber and respective composite. Binder associated with the fibers is influenced by the fiber microstructure, and a continuation of structure is developed throughout the composite body. Even though the fiber fraction is only approximately 50% of the composite by weight, it is clear that fiber microstructure influences overall composite microstructure and, hence, composite physical properties and subsequent composite gasification behavior.

Key Words—Carbon/carbon composites, gasification, PAN fibers, pitch fibers, reactivity.

1. INTRODUCTION

Composites, in general, have long been appreciated as substitutes for conventional materials when the need for superior properties exists in an application. Carbon fiber reinforced carbon composites (C/C composites) are of current interest because of the variety of unique engineering properties they possess. The fiber imparts strength, stiffness and fatigue resistance to the composite, while the carbon matrix holds the fibers together. There is also a synergistic effect between fiber and carbon matrix which results in high fracture toughness and wear resistance. The most attractive properties of composites, however, are their high specific strength and modulus which are the result of the high degree of anisotropy in the graphite crystal lattice.

One of the many uses for these 3D C/C composites is as the exit nozzle for rockets. In this application the composite is subjected to severe conditions produced during solid propellant combustion. During the firing, an oxidative environment is produced; and the composite nozzle gasifies. This is a problem to rocket motor designers, because as the nozzle gasifies, the properties and performance of the motor are altered. Under the extreme conditions which exist in this aerospace application, the C/C composite must maintain predictable design properties. Therefore, the reactivity behavior of C/C composites needs to be predicted for the given operating conditions, prior to actual motor firing.

Towards this end, this investigation was initiated as a first approach to relate the composite fabrication process, the microstructure and physical properties, and their influence on composite gasification behavior in steam. Steam was chosen because it is the single most important species in the gas stream which contributes to C/C composite nozzle gasification in rocket motors propelled by aluminized solid propellants.

2. EXPERIMENTAL APPROACH

2.1 *Materials*

The four C/C composites examined were obtained from the Air Force Rocket Propulsion Laboratory (AFRPL); their intended use was as rocket nozzle materials. All are 3D carbon fiber reinforced composites. Their apparent differences are due to fiber type used and total number of densifications experienced during fabrication.

Table 1 highlights the major compositional differences between each of these composites and gives final bulk densities. The carbon fibers manufactured by Union Carbide Corp., are derived from either polyacrylonitrile (PAN) or coal tar pitch. The carbon matrix is formed from both a coal tar pitch and a thermoset resin. The composites are densified, first by the pitch for a total of three impregnations and then by the resin for additional impregnations.

2.2 *Sample preparation*

Considerable emphasis was placed on accurately sampling the 3D cylindrical C/C billets in a manner which most represented the composite integrity as a rocket nozzle material. However, variations in the fiber fraction of the materials do exist in the billet; and the samples were, therefore, taken from regions where the volume fraction of fibers was highest. Such areas are also those which experience gasification under rocket motor operating conditions.

Samples were removed using a small diamond saw and washed in methanol using an ultrasonic bath. Composite samples, 0.318 cm × 0.635 cm × 0.159 cm, were used for all characterization studies unless otherwise stated. Sample plates contained bundles of fibers lying perpendicular to their faces. Samples prepared for reactivity studies were cut in a similar orientation, and had dimensions 0.318 cm × 0.953 cm × 0.079 cm.

Table 1. Characteristics of C/C composites

SAMPLES	FIBER	DENSIFICATION CYCLES	BULK DENSITY (g/cc)
A	PAN	9	1.96
B	Pitch	6	1.99
C	Pitch	7	1.87
D	PAN	12	1.88

Table 2. Measured properties of C/C composites

	C	B	D	A
Surface Area (m^2/g)	0.19	0.18	0.13	0.10
L_c (nm)	13	32	45	48
L_a (nm)	15	140	100	140
Interlayer Spacing (nm)	0.3422	0.3361	0.3363	0.3361

2.3 *Procedures*

Descriptions of all experimental procedures are given in detail elsewhere[1].

2.3.1 *Specific surface areas.* Determination of total surface area (TSA) was accomplished using the BET theory and Kr as the adsorbate. Six sample slices for each composite were weighed and placed into a sample holder.

2.3.2 *Crystallite size determination.* Sample slices of each composite were ground to -100 mesh. The entire sample (fiber and binder) was ground to this mesh size without sieving. Samples of the ground material (0.05 g) were mixed in a 50:50 ratio by weight with a Si powder standard. The resulting mixture was placed on a glass slide and mixed thoroughly with collodion to bind the sample as a thin film to the glass surface. Three slide mounts of this type were prepared for each composite and examined using a Rigaku X-ray diffractometer with monochromatic (40 KV, 20 mA) CuK_α radiation.

2.3.3 *Density and porosity analysis.* Open, closed and total porosities were calculated directly from experimentally determined, He, Hg, and X-ray densities, using standard procedures.

2.3.4 *Optical microscopy.* Two sample slices in orthogonal orientations were removed from each composite. They were mounted in a thermosetting resin and finely polished repeatedly to remove scratches from the surface. Examination was carried out under polarized light. A half-wave plate was placed between the sample and the analyzer to generate reflectance interference colors.

2.3.5 *Scanning electron microscopy.* All composites were examined in the SEM using 25 KV accelerating voltage, with no conducting metallic layer applied.

2.3.6 *Thermal gravimetric analysis.* The reactivity of each composite was determined in 3.1 kPa of steam carried by N_2 (ultra high purity 99.999% N_2) using a TGA apparatus. The reaction temperature was 1123 K and the gas flow rate was 355 cc (STP)/min. The temperature was controlled to ± 1 K for the duration of each run.

3. RESULTS

3.1 *Surface areas*

Krypton adsorption surface areas are listed in Table 2. Surface areas for the composite materials under examination are quite small, ranging from 0.10 to 0.19 m^2/g. Although this is an extremely narrow range, the composites fabricated with the PAN fibers had smaller surface areas than those containing pitch fibers. Values for the Kr surface areas of the fibers present in the composite have appeared in the literature. Hoffman and Lowry gave a range of surface areas for these fibers between 0.3–0.4 m^2/g[2]. Walker *et al.* reported the surface area of the PAN fiber as 0.37 m^2/g[3]. This agrees well with the geometric area for this fiber, calculated from its outer diameter of 7 μm and a bulk density of 1.71 g/cc.

3.2 *Crystallite parameters*

Figure 1 presents X-ray diffraction patterns for the as-received fibers, prior to composite fabrication and final heat treatment. It is seen that the PAN fibers had a much smaller crystallite size than did the pitch-based fiber. The interlayer spacing of the as-received pitch fiber was 0.343 nm.

Crystallite dimensions and interlayer spacings for the composites are listed in Table 2, the latter being a good indication of the extent of graphitization in each sample. Composites A and B have the smallest interlayer spacings. The interlayer spacing for a perfect graphite crystal

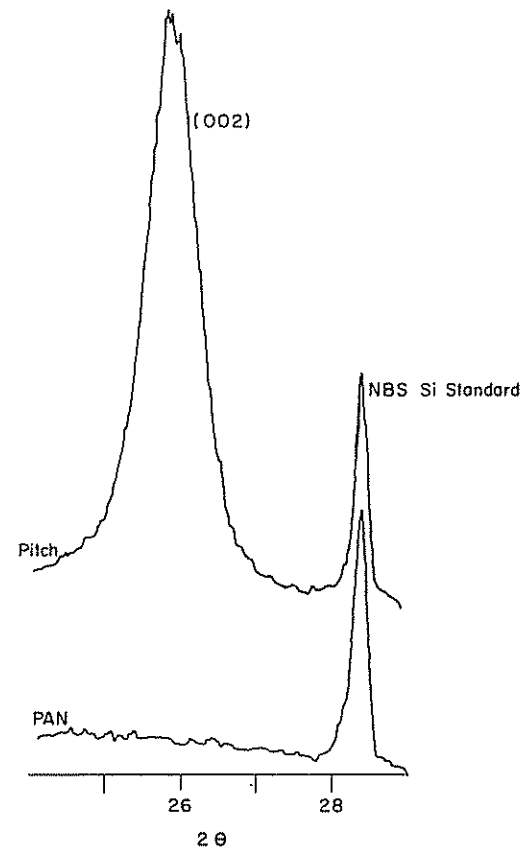

Fig. 1. Diffraction patterns of as-received PAN and pitch fibers.

is 0.33538 nm. A value of 0.3361 nm indicates that these composites (at least the binder carbon in the case of composite A) are well graphitized, since they approach this value. It is apparent that the composite C is poorly graphitized, having a layer spacing of 0.3422 nm. Crystallite parameters for C are also not comparable to those of the other composites.

The d-spacings recorded for the composites are a reflection of the most graphitic constituent present, as long as it is present in reasonable amounts. Since the d-spacings of the C/C composites were determined from a fine powder consisting of fibers, binder and resin, the most graphitizable of these three constituents will produce the dominant diffraction pattern. The interlayer spacings for all the composites, with the exception of C, are approximately 0.336 nm, meaning that at least one phase in each of these composites has a similar degree of crystallinity. As will be shown from microscopy studies, the resin carbon is amorphous and thus cannot be responsible for the pronounced (002) diffraction peak in three of the composites. Further, since PAN is not as graphitizable as coal tar pitch[4], it is thought that the d-spacings recorded for composites A, B and D are representative of the carbon derived from coal tar pitch.

3.3 *Elemental analysis*

A semi-quantitative spectroscopic analysis of trace inorganic elements present in the C/C composites is given in Table 3. B is relatively clean compared to the other samples. No trends in the concentrations of specific elements are evident, although Fe, Si and Ca are generally the predominant trace elements. The presence of trace elements in composites may be primarily the result of sizing the fibers to induce greater adhesion with the matrix. However, we are not aware of any specific treatments to either the PAN or the pitch fibers.

Table 3. Spectrographic analyses of C/C composites

ELEMENTS (ppm)	A	B	D	C
Fe	100	5	40	100
Si	200	50	250	100
B	40	10	40	20
Cu	10	ND	10	100
Ca	100	10	80	100
Mg	40	5	50	500
Mn	10	ND	ND	20
Cr	20	ND	ND	20
Ni	20	ND	ND	20
Co	20	ND	ND	20
V	10	ND	ND	10
Ba	30	ND	ND	30
Sr	5	ND	ND	5
Zr	ND	ND	40	20
Ti	ND	5	20	ND
Al	ND	10	ND	ND

ND - Not Detected

Table 4. Densities and porosities of C/C composites

	C/C Composites			
Properties	A (PAN)	B (PITCH)	C (PITCH)	D (PAN)
Bulk Density (g/cc)	1.96	1.99	1.87	1.88
ρ_{Hg} (g/cc)	2.016	2.042	1.987	1.989
ρ_{He} (g/cc)	2.125	2.171	2.136	2.239
$\rho_{x\text{-ray}}$ (g/cc)	2.263	2.263	2.223	2.262
Open Porosity (cc/g)	0.025	0.029	0.035	0.056
Closed Porosity (cc/g)	0.029	0.019	0.018	0.005
Total Porosity (cc/g)	0.054	0.048	0.053	0.061
Open Porosity (%)	5.1	5.9	7.0	11.2

3.4 *Density and porosity measurements*

Helium, mercury and X-ray densities are presented in Table 4. Also given in this table are total, open and closed porosities as calculated from the density measurements. Percentages of the sample volumes which are accessible to He (% open porosity) are quite small. Composite D has the greatest value (11.2%). The other samples have open porosities which range between 5.1 and 7.0%. Contributions of open and closed porosity to total porosity vary from composite to composite. The smallest amount of closed porosity is present in the D composite. This sample experienced twelve densification cycles, more than the number received by the other composites.

3.5 *Optical microscopy*

In each composite all three carbonaceous constituents are unique and readily identifiable. Porosity (open and closed) is observable, and the degree of adhesion at the fiber/binder interface is also recognizable. Fibers are clearly visible under the microscope. Their structure as filaments is unique. The carbon from the coal tar pitch binder was distinguishable because of its optical activity, displaying reflectance interference colors under polarized light. Thus large domain regions existed in which crystallite alignment was excellent. Carbon derived from the resin could be distinguished since it exhibited no optical activity, indicating random crystallite alignment.

Figure 2 is an optical micrograph which clearly shows the three constituents in composite D. Pitch binder is the closest to the fiber since it was the first impregnant used during densification. Pitch can be seen between both those fibers lying parallel and those lying perpendicular to the plane of the photograph (Fig. 3). Resin is primarily located in pockets in the pitch which may be as large as 25 μm (Fig. 2).

The porosity and porosity distribution in these composites vary because of the number of impregnations

experienced during the densification process. Porosity in these composites is found almost everywhere. Voids exist between the individual fibers in a bundle, around the fiber bundles, at the fiber/binder interface, and at larger structural cracks produced as a result of the processing cycles.

Composite C cracked catastrophically during processing and does not have as graphitic a character as do the other composites in this study. Figure 4, an optical micrograph of this material, shows large thermal stress cracks which are present at regular intervals along the fibers. Also present are separations between the pockets of resin, coal tar pitch, and fiber.

The strength of the fiber/binder interface is of considerable importance in that it underscores the strength of the entire composite billet. Areas of binder pulling away from the fiber are observed in all composites, as well as areas at which the interface is uninterrupted.

3.6 *Scanning electron microscopy*

Each composite can readily be distinguished under the SEM due to the separate and unique microstructure of each fiber type.

Cross-sectional ends of both PAN and pitch fibers are shown in Figs. 5 and 6. PAN fibers have an extremely irregular outer surface with a diameter of approximately 5–6 μm. They appear to have a thin sheath associated with each fiber, but this could be a part of the binder. The crenellated outer surface of the PAN fibers has ridges running parallel to the fiber axis (Fig. 7). Also associated with the PAN fibers are scales which are perpendicular to the fiber axis. These scales are binder material which is intimately associated with the fiber (Fig. 8).

Pitch fibers have an entirely different structure. They have an almost circular cross-section with a diameter of 8–10 μm (Fig. 6). This allows for a close packed fiber stacking which maximizes fiber volume. Between each of the fibers, one can see binder pulling away from the outer surface. There are also cracks in this binder which lie parallel to the fiber axis. The surface of the pitch fiber is completely smooth. In Fig. 9 sheets of the outermost layers are removed in a manner that has the appearance of a roll of paper which is being unwound. Again, it is difficult to say whether this outer sheathing is a part of the binder or the fiber itself. Examination of a single pitch fiber (Fig. 10) shows a microstructure which is composed of many microfibrils, approximately 500 nm in diameter. The sheathing is torn away from the fiber surface, exposing the microfibrils which also have a circular cross-section.

Finally, the binder associated with the fibers has a structure which is almost a continuation of the fiber microstructure. Binder surrounding the PAN fibers has swirl cracks in it, which indicate a mesophase transition having occurred during fabrication (Fig. 11). Binder areas associated with the pitch fibers do not display these cracking patterns. This binder is almost sheet like in nature with some stress cracking present (Fig. 12).

3.7 *Composite reactivity*

Reactivities of the 3D C/C composites are given in Fig. 13. Shown are burn-off versus time plots for the four composites at 1123 K with a 3.1 kPa entering steam pressure. There are two distinct sets of burn-off curves for the four samples. Samples D and A are roughly three times as reactive under the experimental conditions used as are samples C and B. The former two composites are fabricated from PAN fibers, while the latter are made from pitch fibers.

Figure 14 is an expanded view of these reactivity plots at low levels of burn-off. Initial rate data follow the same trends seen in the extended reactivity plots. Composites made from PAN fibers are more reactive than those made using pitch fibers. The steady state rates (rates taken over the linear portion of the extended burn-off plots) for each composite are presented in Table 5. These rates are expressed in two different sets of units—mg reacting per h per mg starting weight and mg reacting per h per m^2 starting Kr surface area (TSA). Rates expressed by the first unit differ by a factor of 3.1; rates expressed by the second unit differ by a factor of 5.5. Rates are also given for two of the composites normalized to active surface area (ASA). They will be discussed shortly.

4. DISCUSSION

4.1 *SEM and optical results—relevance to physical properties*

Composites fabricated with pitch fibers have larger surface areas as measured by Kr adsorption at 77 K than do the composites fabricated with PAN fibers. Visible details of the composite microstructure provide an explanation. The composites containing pitch fibers have cracks in the binder area which are as large as 500 nm. Cracks in this area run parallel to the pitch fiber axis. Porosity developed as a result of this cracking is accessible to Kr, and its presence increases the surface area of the composite. Composites which are composed of PAN fibers do not exhibit open porosity of the same degree. Binder does not shrink and pull away from the PAN fiber surface as it does with the pitch fibers. Instead, there is scale development of the binder perpendicular to the PAN fiber axis which inhibits the growth of open porosity along the fiber length. Graphitic layers of binder act as plates, closing off accessible porosity. This binder structure does, however, create a more developed closed porosity.

Figures 11 and 12 are micrographs of the binder areas in composites containing PAN and pitch fibers, respectively. The orientation of the micrographs is parallel to the fiber axis. Swirl cracks in the binder associated with the PAN fiber give rise to the scale development seen on the PAN fibers. Scales are the result of shear stresses on the binder area when PAN fibers in the composite were physically separated for observation. Development of mesophase lamellae within the binder of composites fabricated with PAN fibers had orientation to the fiber axis which was not expected. Lamellae of the mesophase normally orient parallel to the fiber surface, resulting in basal planes in the binder juxtaposed parallel to the fiber surface. Here instead, the mesophase lamellae are oriented perpendicular to the fiber surface and maintain this orientation throughout the processing. Thermal stresses develop the swirl cracks between graphite layer planes in

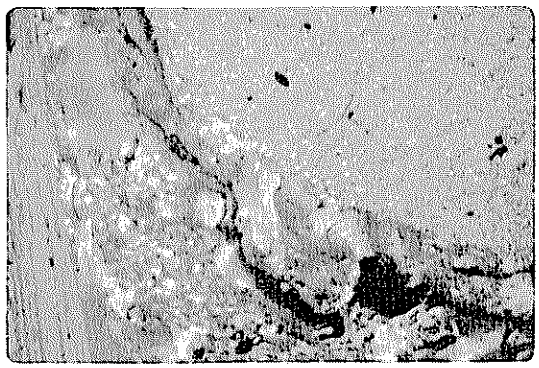

Fig. 2. PAN fiber, pitch carbon and resin carbon in composite D.

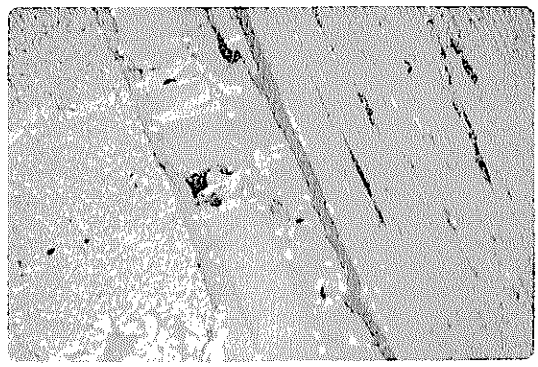

Fig. 3. Location of pitch binder and resin impregnant with respect to supporting fiber and axial fibers composite D. Note cracking in the binder.

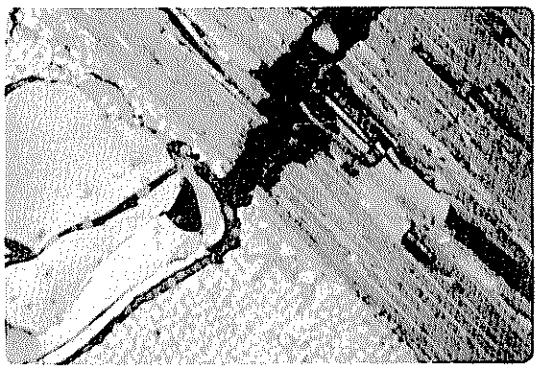

Fig. 4. Cracking in supporting fibers and surrounding resin impregnant. Composite C.

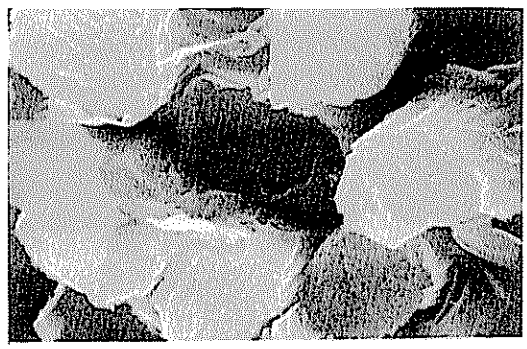

Fig. 5. PAN fiber cross-section, composite A.

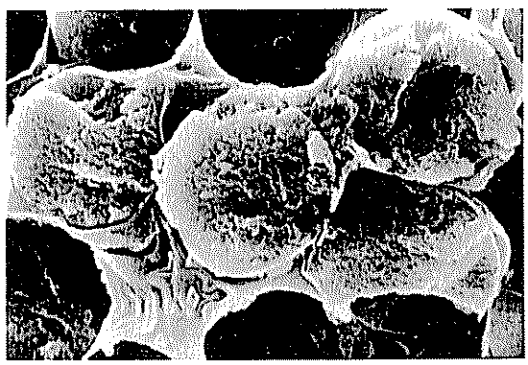

Fig. 6. Pitch fiber cross-section, composite B.

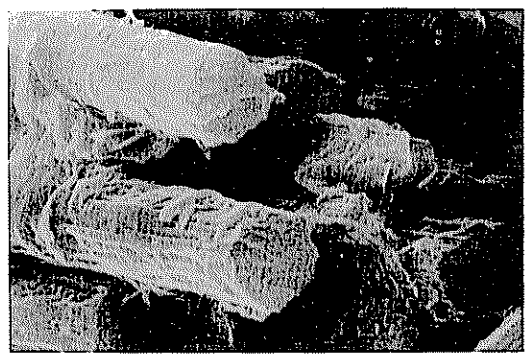

Fig. 7. PAN fiber surface showing ridges along fiber axis, composite A.

the binder which become closed porosity inaccessible to either Kr or He. A greater amount of closed porosity is consistent with PAN-based fiber composite A having a greater porosity closed to He and a lower Kr surface area than does the pitch-based fiber composite B, as seen in Tables 2 and 4. Smooth and regular flow patterns of binder associated with pitch fibers reflect the parallel orientation of this binder to the fiber axis. The continuation of structure from the pitch fibers is a concentric arrangement of binder carbon layer planes around the smooth and cylindrical pitch fiber axis. Separation of pitch fibers from the composite billet cleanly shears the binder basal plane from the fiber basal plane (running along the fiber axis). This binder area is shown in Fig. 12. Depressions remain in areas where fibers were removed. Stress fractures shown are the result of some irregularities in the processing of this composite.

It is interesting that all four composites have similar levels of total porosity; however, the amounts of open and closed porosity vary. Stress cracks may develop within

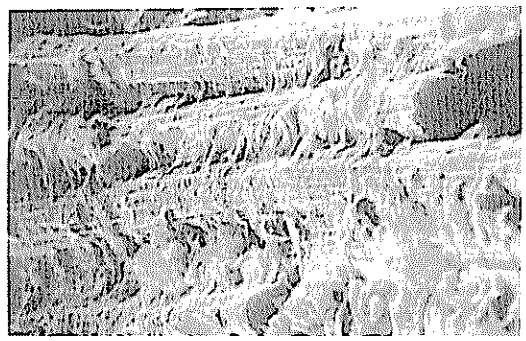

Fig. 8. Scales on PAN fiber surface, composite A.

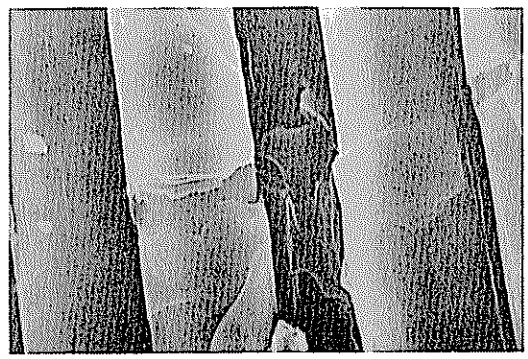

Fig. 9. Outer surface of pitch fiber, composite B.

Fig. 10. Pitch fiber containing microfibrils, composite B.

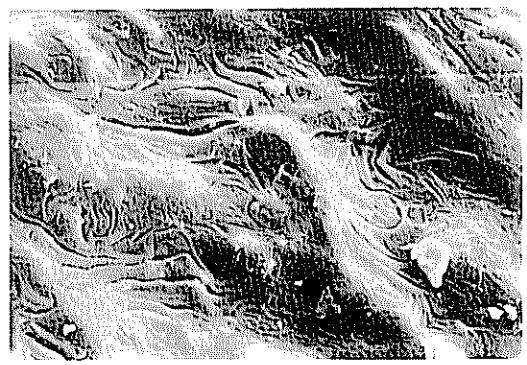

Fig. 11. Binder associated with PAN fiber composite A.

Fig. 12. Binder associated with pitch fiber composite B.

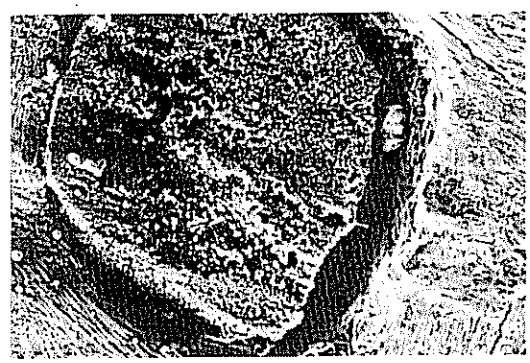

Fig. 15. Actual recession of PAN fiber end below the composite surface on a post-fired rocket nozzle composite D.

composites containing pitch fibers, giving rise to the closed porosity of these composites. Development of stress cracks in anomalous billets can eventually reduce the amount of closed porosity and increase the level of open porosity contained by the composite. This is the case with composites D and C; large stress fractures were seen in both fiber and binder. Because of this, composite D has 92% of its total pore volume accessible to He; whereas composite A, which had no processing anomalies, has only 46% of its total pore volume accessible to He.

Finally, both types of carbon fiber contain porosity due to the orientation of the non-planar "graphitic" layers (fibrils) of which they are composed. This orientation, which has been described using a "wrinkled ribbon" model, places these fibrils generally with alignment parallel to the fiber axis[5]. Elongated pores in the range of

1–2 nm in diameter and 20 nm in length exist between these interwoven fibrils. Examination of the pitch fibers has provided evidence of the existence of fibrils within the fiber structure. The accompanying porosity is inaccessible due to the "sheathing" of these fibers in a skin which appears to be part of the fiber itself. In Fig. 10, the sheath is pulled away from the pitch fiber, exposing fibrils. Porosity of this sort contributes to the closed porosity of these composite materials.

4.2 *Composite reactivity.*

4.2.1 *Influence of impurities on reactivity.* Impurities have a profound influence on the gasification of carbonaceous materials in steam. It is well recognized that Fe, Co, and Ni catalyze the carbon-steam reaction[6]. These trace elements are present at different levels in each of the composites. Calcium is also an excellent catalyst for carbon gasification in steam. However, due to the complexity of studying catalytic activity and the number of possible catalysts present, a detailed investigation was not conducted. No obvious correlations were drawn between specific elements and their catalytic activity in C/C composite gasification by steam.

4.2.2 *Active surface area—normalization of composite rates.* Rates measured on each composite can be normalized in several different ways. Table 5 lists these rates under experimental conditions, normalized to initial sample weight and to TSA measured by Kr adsorption. It is not surprising that attempts to normalize reactivities based on TSA are not successful, based on the large difference in reactivities of the basal plane and prismatic planes in graphite. Physical adsorption of Kr does not differentiate between these surfaces. A better normalization of these data should be possible, however, using total active surface area (ASA) as measured by oxygen chemisorption[7].

Oxygen chemisorption measurements are based on oxygen atoms chemisorbing on carbon sites occupying 0.083 nm^2 at the edges of carbon crystallites (prismatic planes). A and B were selected for this study. Details of the experimental procedures are described by Taylor[8]. Sample slices, as used in all other characterization experiments, were brought to 573 K in 66.4 Pa of O_2 for 24 h. The amount of oxygen chemisorbed was determined directly from the amount of CO and CO_2 desorbed upon subsequent heating of the samples at 1233 K in vacuum. The ASA's were 0.14 m^2/g and 0.63 m^2/g for B and A. It is interesting that the ASA for composite A measured at 573 K greatly exceeds its TSA, as measured by the physical adsorption of Kr at 77 K. Taylor recognized that there is some uncertainty in the area to be assigned to a chemisorbed oxygen atom[8]. He assumed that all the oxygen was bonded to the carbon surface in carbonyl groups, in which case an assigned area of 0.083 nm^2 is reasonable. However, if oxygen were bonded in anhydride groups, for example, one oxygen atom would occupy only about 0.054 nm^2. In any case, no reasonable bonding of oxygen in a functional group would lower the area occupied by the oxygen atom sufficiently to reduce the ASA for composite A below that of its TSA. The conclusion is that at 573 K, O_2 is accessible to some microporosity which is inaccessible to Kr at 77 K. This is not surprising for two reasons. First, O_2 has a smaller minimum dimension than does Kr. Second, the higher the measurement temperature, the greater the value of the diffusion coefficient; and the more rapidly equilibrium is attained. It was pointed out earlier that composite A has a larger closed pore volume than does B. This is consistent with the discrepancy between ASA and TSA being greater for composite A.

Table 5. Rates of reaction for 0.079 cm thick sample slices at 1123 K in 3.1 kPa steam

SAMPLES	RATE (mg/mg-h)	RATE (mg/m^2 TSA-h)	RATE (mg/m^2 ASA-h)
A	0.018	180.0	28.6
B	0.014	107.7	---
B	0.0059	32.8	42.1
C	0.0083	43.7	---

Table 5 presents reactivity results for A and B normalized by the ASA. The rates differ by a factor of 1.5. This difference could be attributed to at least two factors. Overall reactivities are the sums of an uncatalyzed rate and a catalyzed rate. In the case of the uncatalyzed rate, O_2 dissociates at carbon active sites. However, in the case of the catalyzed rate, O_2 dissociates (and more efficiently) at impurity sites. The contributions of the catalyzed rates to the overall rates for the two composites could (and would be expected to) be different depending upon the specific activities of impurities present and their degree of dispersion. Second, steam at reaction temperature (1123 K) would be expected to be more accessible to previously assigned closed pores than would O_2 at 573 K. In this case ASA, as measured by oxygen chemisorption at 573 K, would still not be expected to be a precise normalizing parameter, even if the contributions of the catalyzed rates to the overall rates happened to be negligible.

The measured ASA takes account of the anisotropy of the graphite structure, being located primarily on the edges of basal planes. Due to the weave of the fibers in the composite, a large amount of the exposed composite surface is composed of fiber surfaces. The alignment of basal planes near the outer surface of a fiber is preferentially circumferential, i.e. they are arranged in concentric cylinders, not in radial directions. Therefore, the exposed portion of these fibers consist of basal plane surfaces, containing little ASA. The remainder of the composite surface is binder and some fiber ends.

Binder areas are influenced heavily by the amount of porosity they contain. Fiber ends are mostly located on the surface of the composite and are readily accessible to the propellant product stream. The edge area of the fiber crystallites contains most of the fiber ASA, and this edge area is located at the ends of the fibers. Under rocket motor operating conditions, these fiber ends erode much more rapidly than the surrounding composite material[9]. Pock marks are produced on the C/C surface as evidence of the concentrated active area at these sites (Fig. 15). It is this fiber edge area, along with accessible binder

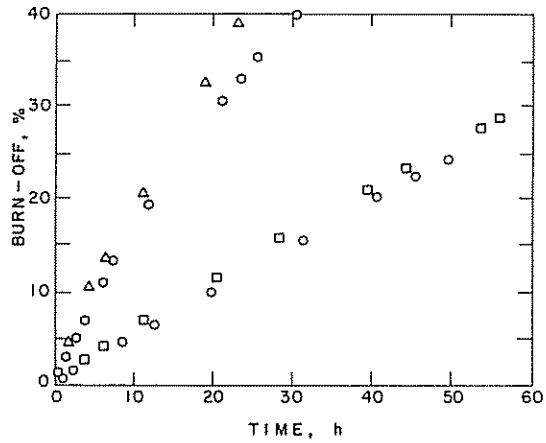

Fig. 13. Reactivities of composites in 3.1 kPa entering H_2O at 1123 K: ○, B; □, C; ◯, D; △, A.

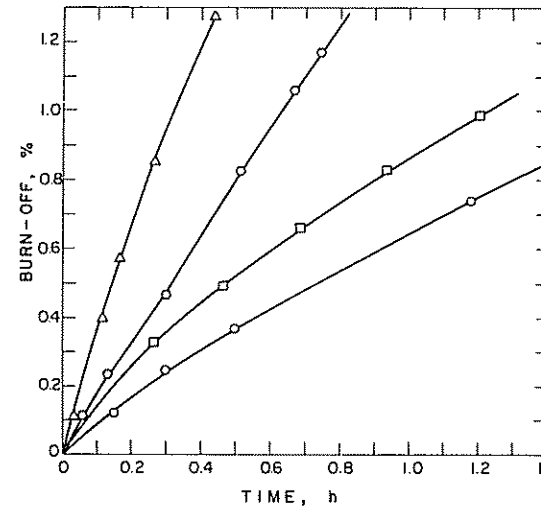

Fig. 14. Initial burn-off vs time plots at 1123 K in 3.1 kPa entering H_2O for composites: △, A; ◯, D; □, C; ○, B.

edge area which contain the measured ASA; and it is this area which appears to reflect the observed recession results.

4.2.3 *Preferential reactivity of specific carbonaceous constituents*. Each composite is composed of three uniquely identifiable constituents, viz. the fibers, the coal tar pitch binder carbon, and the resin carbon. Each of these has a unique structure and associated reactivity. As described, the fiber should gasify preferentially at the fiber ends, where edge area is concentrated. The only exception to this would be gasification at vacancies or dislocations on exposed fiber basal surfaces.

Pitch binder carbon is graphitizable and exhibits reflectance interference colors indicative of graphitic layer plane development and alignment. Reactivity of this binder area would depend on the degree of layer plane development during the mesophase transition and the creation of these lamellae. Yet, more important is the accessibility of binder area to the reactant gas species.

The resin carbon is amorphous and has the appearance of a glassy carbon, which has a randomly oriented crystallite structure. Precursors of glassy carbons are usually thermosetting resins. The amorphous appearance of this material is the result of very little crystallite growth and a system of cavities and apertures created by its disordered crystallite structure. One might, therefore, predict a higher reactivity for this resin carbon than for the pitch binder carbon. However, a unique physical property of glassy carbons is their impermeability to gases. Most of the porosity they contain is not accessible, resulting in very small available surface area. All of this would combine to produce a material which would not necessarily be more reactive than the pitch binder carbon.

As expected, it is found that gasification rates of glassy carbon artifacts are uniform in the different orthogonal directions[10]. Whether the overall gasification rate of the artifact is higher or lower than that of graphite artifacts depends upon the ratio of basal plane to edge surface area in the latter. For a high ratio, glassy carbon has the higher reactivity; for a low ratio, graphite artifacts have the higher reactivity[10].

5. SUMMARY

It is evident that gasification behavior is directly linked to the structure of the fiber constituent in these C/C composites. Fiber structure appears to dictate the amount of accessible porosity to corrosive gases in these materials by influencing the development of the associated binder phases. Perhaps, this is most apparent with the composites composed of pitch fibers which have a circular cross-section and smooth outer surface. Binder wraps itself around these fibers in a concentric fashion during the densification process; and, as a result, the ASA of these composites is concentrated at the fiber ends.

The development of composite microstructure is not as obvious for the composites fabricated with PAN fibers. Their structure is irregular, having a crenellated cross-section and a roughened outer surface. Binder forms scales on this fiber surface which lie perpendicular to the fiber. The reason for this development is not obvious but may possibly be attributed to processing. Perhaps, a pressure treatment of these composites during processing coupled with the unique structure of these PAN fibers influences this scale formation. These scales of binder still attached to the PAN fiber surface indicate that this fiber/binder interface is much improved over that of the pitch fiber/binder interface. Strength of a composite depends greatly upon the extent of bonding at the interface between binder carbon and fiber surface.

In this study composites composed of PAN fibers are more structurally sound based on this interface. However, their ASA and subsequent mass reactivity are greater. Therefore, one must understand the structural tradeoffs to be made between mechanical properties and gasification behavior when using composites composed of uniquely structured fibers.

Acknowledgement—This research was conducted under Contract F04611-81-K-0067, sponsored by the Air Force Rocket-Propulsion Lab, Edwards Air Force Base, CA.

REFERENCES

1. L. E. Jones, M.S. thesis, The Pennsylvania State University (1984).
2. W. P. Hoffman and J. A. Lowry, *Abstracts 16th Biennial Conf. on Carbon*, San Diego 357–358 (1983).
3. P. L. Walker, Jr., T. A. Eapen, I. M. Ismail and O. P. Mahajan, TANSO **108**, 2 (1982).
4. L. S. Singer, *Int. Symp. on Carbon*, Toyohashi, Japan, 400 (1982).
5. A. Fourdeux, R. Perret and W. Ruland, *Proc. 1st Int. Conf. Carbon Fibers*, London, 57 (1971).
6. D. W. McKee, *Carbon* **12**, 453 (1974).
7. N. R. Laine, F. J. Vastola and P. L. Walker, Jr., *J. Phys. Chem.* **67**, 2030 (1963).
8. R. Taylor, Ph.D. thesis, The Pennsylvania State University (1982).
9. L. E. Jones, P. L. Walker, Jr., P. A. Thrower and K. K. Kuo, AFRPL Final Rep. Edwards AFB, CA, F04611-81-K-0067 (1985).
10. F. Rodriquez-Reinoso and P. L. Walker, Jr., *Carbon* **13**, 7 (1975).